Chapter 3

On an Overview of Nonlinear and Chaotic Behavior and Their Controls of an Atomic Force Microscopy (AFM) Vibrating Problem

José Manoel Balthazar, Angelo Marcelo Tusset, Atila Madureira Bueno and Bento Rodrigues de Pontes Junior

Additional information is available at the end of the chapter

http://dx.doi.org/10.5772/51834

1. Introduction

It is known that in Brazil and in the whole world, the development of mathematical modeling techniques for the study of problems involving new technologies and the design of nonlinear structures is an emerging area in Engineering Science. To background to the general problems of non-linear dynamics, see the comprehensive monographs: (Awrejcewicz, 1991) and (Awrejcewicz and Lamarque, 2003).

This chapter addresses this issue, involving the dynamical behavior of Electrical Mechanical Systems (EMS), that are systems responsible for electromechanical energy conversion. It is common knowledge that an electromechanical system can be classified in three different groups, according to scales dimensions: *i*) Macro-Systems >1mm, *ii*) Micro-Systems <1mm and >0.1μm, and *iii*) Nano-Systems <0.1 μm and >0.1nm.

The Macro-Systems are characterized by being visible without using microscope and they are present in our Day to Day activities. The Micro-Systems are generally constructed on silicon chips, and are employed in manufacturing integrated electronic circuits. The Nano-Systems can only be seen and manipulated with the use of the Atomic Force Microscope.

In this research field - MEMS and NEMS -, the researches are based on the fact that, in opposition to traditional macro-scale problems, the atomic forces effects and surface phenomena are preponderant over the forces of inertia and gravity. It is also known that the manufacture of these new products have been based on the binomial consuming time and an enormous amount of financial resources. Thus, it becomes necessary some investment in an interface, which addresses the design and manufacturing that, gives designers of

"MEMS" and "NEMS" the proper tools of mathematical modeling and simulations as well as qualitative dynamic analysis. It should be considering a macro-model, which agrees with the simulation results on a physical level, and with the experimental results, obtained from test structures in a lab. Many surveys have been developed in major research centers in Brazil and throughout the world in this direction. It is announced that several research groups in Brazil are involved with this theme, but most of the research carried out or in development focuses on experimentation or in the use of the numerical method - called finite element method. It is known that the nonlinear phenomena are prevalent in MEMS and NEMS, which is a strong motivation for the work of our research group.

The main idea of this chapter lies in the study of "State of the Art" of non-linear dynamic models and the design of their controls, since this new area of research is of paramount importance. This chapter deals with two boundary problems belonging to this line of research, in development at the university of Rio Claro and Bauru UNESP, for us, through research groups and development projects for Graduate (Masters) and Post–Doctor. Mainly for the Atomic Force Microscope.

2. General aspects of the Atomic Force Microscope (AFM)

In Binnig et al. (1986) the atomic force microscope ("AFM") was presented. The AFM has been described as one of the most efficient tools for obtaining high-resolution images of the samples, by exploiting its surface, both in air and in liquid media. At the core of the "AFM", there is a tip, mounted on the end of a micro cantilever, while the tip vibrates to scan the sample, its vibration is detected by a laser system, which emit signals to a photo detector that generate images of the object under examination at high resolution. This movement may vary depending on the need and on the type of material being analyzed. These variations include techniques such as static contact mode and dynamic techniques, such as non-contact mode and intermittent or tapping mode. The principle of operation of the "AFM" is to the measure the deflection of the microcantilever on whose free end the probe is mounted. The deflections (analyzed during the scan) are caused by forces acting between the tip and sample. These forces act on medium to large distances - typically ≥ 100 Å – such as attractive Van der Waals forces, magnetic forces and Coulomb forces (Eisenschitz, 1930). It can be said that when the tip approaches to the sample, it is first attracted by the surface, due to a wide range of attractive forces in the region. This attraction increases when the probe is very close to the sample. However, when the atoms of the tip and sample become very close, the orbital electrons begin to repel. The forces are canceled when the distance between the atoms is of the order of several angstroms (the distance of the order characteristic of a chemical bond). When the forces become positive, it can be said that the atoms of the tip and the sample are in contact and ultimately the repulsive forces dominate.

In Figures: 1,2 and 3, the main characteristics and the operation of an AFM can be observed. Figure 3; display the basic configuration of an AFM. The micro cantilever is V-shaped or rectangular with a sharp tip. This tip is usually of pyramidal or conical shape (Figure 2).

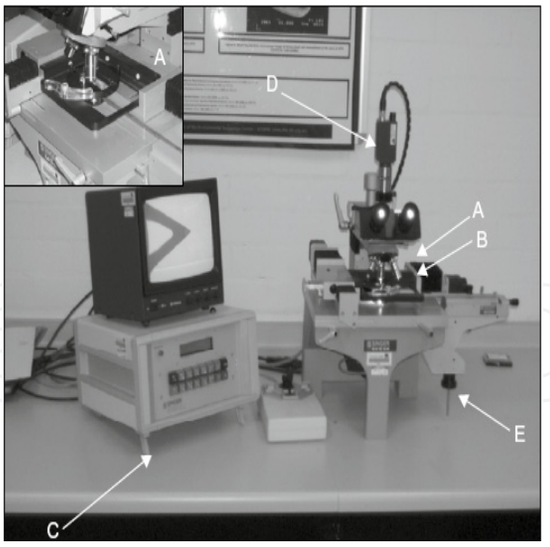

Figure 1. AFM photo (source: Bowen and Hilal 2009)

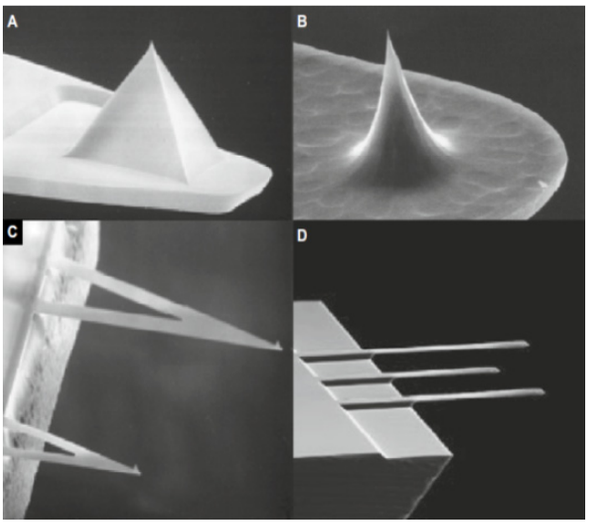

Figure 2. (source: Bowen and Hilal 2009)

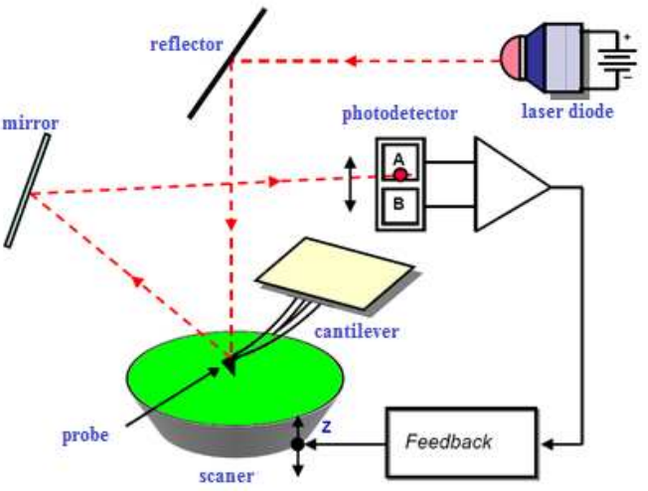

Figure 3. Control of the positioning of the scanner. Adapted from : (Cidade et al. 2003)

Typically, probes are made predominantly of silicon nitride (Si3N4); its upper surface is coated with a thin reflective surface, generally gold (Au) or aluminum (Al). The probe is brought to inside and out of contact with the sample surface, by using a piezo-crystal (Hilal and Bowen, 2009). In the illustration of a typical micro-manipulator, shown in Figure 3, it is possible to observe that it consists of a movable stage mounted under an optical microscope. The movement of the base can be controlled by an electronic control console. Large deflections are required to achieve high sensitivity. Therefore, the spring should be very "soft" (slightly stiff).

2.1. Operation modes in AFM

The probe mounted on the AFM performs the scan on the sample in a raster fashion. The movement of the microcantilever over the sample is carried out by the piezoelectric scanner, which comprises piezoelectric material that expands and contracts according to the applied voltage. There are several modes of operation for scanning and mapping surface. These modes include non-contact, contact and intermittent contact modes. These three modes of operation differ from each other, basically, by the tip and sample distance.

The Lennard-Jones potential describes the relationship of the tip and sample interaction forces as depending on the tip and sample surface distance, considering the potential energy of a pair of particles, and is given by:

$$U(r) = 4\varepsilon\left[\left(\frac{\sigma}{r}\right)^{12} - \left(\frac{\sigma}{r}\right)^{6}\right] \tag{1}$$

where ε and σ are constants depending on the sample properties, σ is approximately equal to the diameter of the particles involved. Deriving potential function (U) in relation to the distance (r) gives an expression for the force (F) versus distance (r) (Equation (1a)). This force is represented in Figure 4.

$$F(r) = -\frac{\partial U}{\partial r} = 24\varepsilon\left[\frac{2\sigma^{12}}{r^{13}} - \frac{\sigma^{6}}{r^{7}}\right] \tag{1a}$$

The region above the r-axis corresponds to the region where the repulsive forces dominate (contact region). The region below the r-axis corresponds to the region where attractive forces dominate (non-contact region). Also in red, it can be seen the distance region that the tapping-mode technique is applied.

3. Mathematical modeling of the Atomic Force Microscope (AFM)

The mathematical models governing the dynamics of the AFM micro-beams, usually result from the discretization of the classical beam equations, based on its mode of vibration, leading to one or more degrees of freedom. Several models of this kind are described in the literature, e.g., Wang et al. (2009), Garcia and San Paulo, (2000); (Laxminarayana and Jalili,

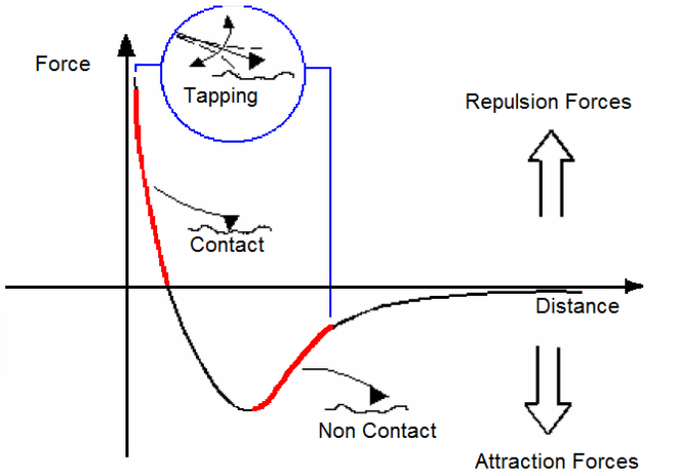

Figure 4. Force (F) versus Distance (*r*), (Source: Cidade et al., 2003).

2004), (Hu and Raman, 2007) (Raman et al. 2008), (Ashab et al. 1999), (Farrokh et al. 2009), (Lozano and Garcia, 2008) among others. Most of the mathematical models are linear mass-spring-damper systems incorporating nonlinear interaction between the tip and sample (Paulo & Garcia, 2002). Different AFM techniques provide a number of possibilities for topographical images of the samples, generating a wide range of information. In this chapter models for intermittent contact mode are discussed.

3.1. Mathematical modeling of AFM: with inclusion of the cubic (spring) term

The physical model of the AFM tip-sample interaction can be considered as shown in Figure 5 (Wang, Father and Yau, 2009). The microcantilever-tip-sample system is regarded as a sphere of radius R_s and mass m_s, suspended by a spring of stiffness $k = k_{l_s} + k_{nl_s}$, where k_{l_s} and k_{nl_s} are the linear and nonlinear stiffness. The van der Waals potential for the sample-sphere system is given by:

$$P = -\frac{A_c R_c}{6(Z_b + X)} + \frac{1}{2}k_{l_s}X^2 + \frac{1}{4}k_{nl_s}X^4 \tag{2}$$

The energy of the system scaled by the mass of the cantilever is given by $E(X, X', Z)$:

$$E = \frac{1}{2}\dot{X}^2 + \frac{1}{2}\omega_1^2 X^2 + \frac{1}{4}\omega_2^2 X^4 - \frac{D\omega_1^2}{(Z_b - X)} \tag{3}$$

Replacing $X_1 = X$ and $X_2 = \dot{X}$, then, from equation (3) results:

$$\begin{aligned} X'_1 &= \frac{\partial E}{\partial X_2} \\ X'_2 &= -\frac{\partial E}{\partial X_1} \end{aligned} \tag{4}$$

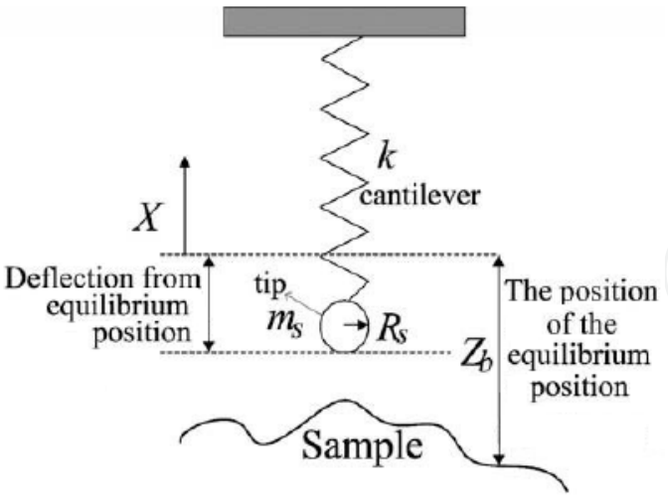

Figure 5. Model of an AFM (Source: Wang, Father and Yau (2009))

The dynamic AFM system in Figure 5 is obtained replacing (2) and (3) into (4):

$$\begin{cases} \dot{X}_1 = X_2 \\ \dot{X}_2 = -\omega_1^2 X_1 - \omega_2^2 X_1^3 - \dfrac{D\omega_1^2}{(Z_b + X_1)^2} \end{cases} \tag{5}$$

where Z_b the distance from the equilibrium position. The molecular diameter is $D = \dfrac{A_H R}{6k}$, where A_h is the Hamaker constant and R is the sphere radius. Considering only attractive Van der Waals force, and that the cantilever is being excited by $mf\cos(wt)$, where w is the natural frequency, the system equations can be written as:

$$\begin{aligned} \dot{X}_1 &= X_2 \\ \dot{X}_2 &= -\omega_1^2 X_1 - \omega_2^2 X_1^3 - \frac{D\omega_1^2}{\left(Z_b - X_1\right)^2} - f\cos wt - \phi X_2 \end{aligned} \tag{6}$$

Where $\phi X_2 = \left(a_4 \cos b - a_5 X_2\right)'$ is the damping force. Considering the relations: $x_1 = \dfrac{X_1}{Z_s}$, $x_2 = \dfrac{X_2}{\omega_s Z_s}$, $z = \dfrac{Z_b}{Z_s}$, $Z_s = \dfrac{3}{2}\left(2D\right)^{\frac{1}{3}}$ and $\tau = wt$, the system (6) may be rewritten in the following dimensionless form:

$$\begin{aligned} \dot{x}_1 &= x_2 \\ \dot{x}_2 &= -a_1 x_1 - a_2 x_1^3 - \frac{b}{\left(z + x_1\right)^2} + c\sin\tau \end{aligned} \tag{7}$$

3.2. AFM Mathematical modeling: intermittent mode and hydrodynamic damping

The microcantilever schematic diagram of the AFM operating in intermittent mode can be seen in Figure 6. The base of the microcantilever is excited by a piezoelectric actuator generating a displacement $f\cos(wt)$. According to (Zhang et al., 2009), considering only the first vibration mode, the (AFM) can be modeled as a spring-mass-damper, as shown in Figure 7. The "tip" is considered as being a of radius R and Z_0 is the distance from the equilibrium position of the cantilever to the sample. The position of the cantilever is given by x, measured from the equilibrium position. According to (Rutzel et al., 2003) the tip-sample interaction can be modelled as a sphere- flat surface interaction, given by:

$$U(x,z_0)=\frac{A_1R}{1260\left(z_0+x\right)^7}-\frac{A_2R}{6\left(z_0+x\right)} \tag{8}$$

where $U(x,z_0)$ is the Lennard-Jones potential(LJ), $A_1=\pi^2\rho_1\rho_2c_1$ and $A_2=\pi^2\rho_1\rho_2c_2$ are the Hamaker constant for the attractive and repulsive potential, respectively, with ρ_1 and ρ_2 the densities of the interacting components, and c_1 and c_2 are constants from interaction. It should be noted that, when the "cantilever" is close to the sample, attractive van der Waals

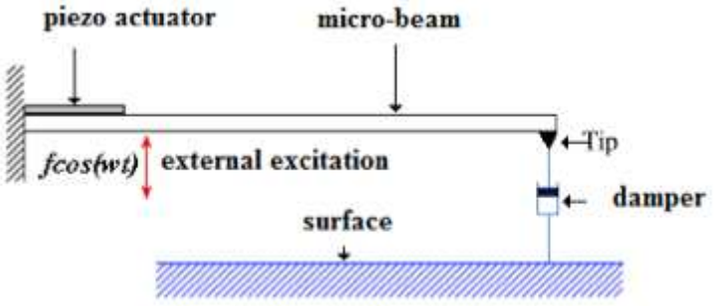

Figure 6. Microcantilver-tip-sample system

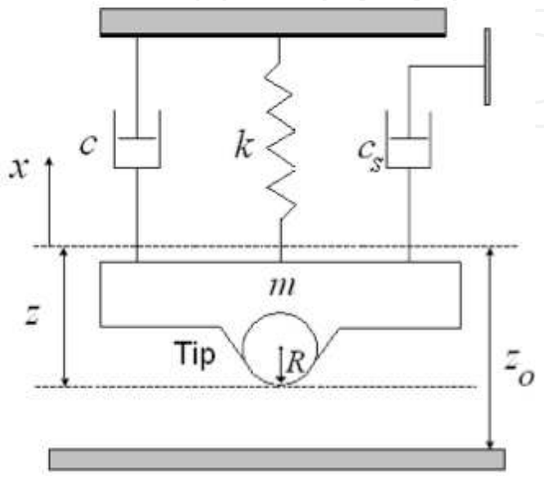

Figure 7. Physical model (Source: Zhang et al., 2009)

force must be considered. These forces can be represented as the sum of the attractive and repulsive forces (Rutzel et al., 2003), expressed by:

$$F = -\frac{\partial U}{\partial(x+z_0)} = \frac{A_1 R}{180\left(z_0+x\right)^8} - \frac{A_2 R}{6\left(z_0+x\right)^2} \tag{9}$$

In the intermittent mode (TM-AFM) the probe touches the surface of the sample at the point of maximum amplitude of oscillation. During the scanning the microcantilever is driven to oscillate according to the force $f\cos wt$, resulting that the tip-sample contact generates the force F. The contact between the tip and sample is delicate, and this mode of operation is suitable for fragile samples. Then, considering the Lagrangian $L = T - V$ and the Euler-Lagrange equation $\frac{d}{dt}\left(\frac{\partial L}{\partial \dot{q}_i}\right) - \frac{\partial L}{\partial q_i} = Q_i$, where

$$T = \frac{1}{2}m\dot{x}^2,\ V = \frac{1}{2}k_l x^2 + \frac{1}{4}k_{nl}x^4 \text{ and } Q_i = F + c\dot{x} + c_s\dot{x} + f\cos wt \tag{10}$$

are the kinetic energy, the gravitational potential energy, and nonconservative forces, respectively, the equation of motion for the microcantilever tip displacement x is given by:

$$m\ddot{x} + c\dot{x} + k_l x + k_{nl}x^3 = \frac{A_1 R}{180\left(z_0+x\right)^8} - \frac{A_2 R}{6\left(z_0+x\right)^2} + \frac{\mu_{eff}B^3 L}{\left(x+z_0\right)^3}\dot{x} + f\cos wt \tag{11}$$

with:

$$c_s\dot{x} = \frac{\mu_{eff}B^3 L}{\left(x+z_0\right)^3}\dot{x} \tag{12}$$

where μ_{eff} is an effective coefficient of viscosity, B the width of the cantilever and L is the length of the cantilever (Zhang et al. (2009)).

Defining:

$$Z_s = \left(\frac{2}{3}\right)\left(2D\right)^{1/3} \tag{13}$$

where $D = \frac{A_2 R}{6k}$ and considering the following relations in (11)

$\tau = w_1 t$, $y = \frac{x}{z_s}$, $\dot{y} = \frac{\dot{x}}{w_1 z_s}$, $a = \frac{z_0}{z_s}$, $b = \frac{k_l}{k_{at}}$, $c = \frac{k_{nl}}{k_{at}}z_s^2$, $d = \frac{4}{27}$, $e = \frac{2}{405}\left(\frac{a}{z_s}\right)^6$, $g = \frac{f_0}{k_{at}z_s}$,

$p = \frac{\mu_{eff}B^3 L}{m w_1 z_s^3}$, $\Omega = \frac{w}{w_1}$, $r = \frac{1}{Q}$. Equation (11) can be rewritten in the dimensionless form:

$$\ddot{y} + r\dot{y} + by + cy^3 = -\frac{d}{(a+y)^2} + \frac{e}{(a+y)^8} + g\cos\Omega\tau - \frac{p}{(a+y)^3}\dot{y} \tag{14}$$

Writing equation (14) into state space form results:

$$\begin{aligned} \dot{x}_1 &= x_2 \\ \dot{x}_2 &= -rx_2 - bx_1 - cx_1{}^3 - \frac{d}{(a+x_1)^2} + \frac{e}{(a+x_1)^8} + g\cos\Omega x_3 - \frac{p}{(a+x_1)^3}x_2 \end{aligned} \tag{15}$$

where: $x_1 = y$, $x_2 = \dot{y}$ and $x_3 = \tau$.

Considering the values of parameters: $\Omega = 1$; $r = 0.1$; $b = 1$; $c = 0.35$; $d = 4/27$; $e = 0.0001$; $g = 0.2$; $p = 0.005$ e $a = 1.6$ (obtained by Zhang et al. (2009)). The displacement can be seen in Figure 8a and the phase portrait can be seen in Figure 8b.

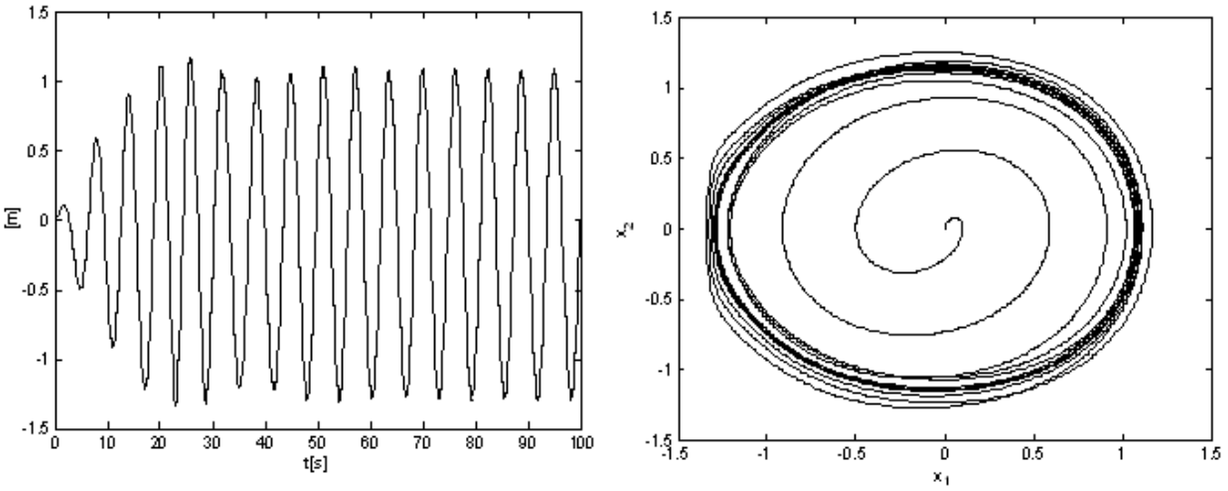

Figure 8. (a): Tip displacement (b): Phase Portrait

4. Chaos in mathematical model with cubic spring

According to Ashhab (1999) the chaotic behavior of AFM depends on the damping of the excitation and on the distance between the tip and the sample, suggesting that a feedback control of the states can be used to eliminate the possibility of chaotic behavior. According to that, considering the system (7) in nondimensional form:

$$\begin{aligned} \dot{x}_1 &= x_2 \\ \dot{x}_2 &= -\alpha a_1 x_1 - \alpha a_2 x_1^3 - \frac{b}{(z+x_1)^2} + \delta\sin\tau \end{aligned} \tag{16}$$

with the parameters: $\alpha = 0.14668$; $b = 0.17602$, $\delta = 2.6364$ e $z = 2.5$, $a_1 = 1$, $a_2 = 14.5$, numerically simulation results can be seen Figure 9. Additionally, The FFT and the Lyapunov exponents ($\lambda_1 = 0.336$, $\lambda_2 = -0.336$) are shown in Figure 10.

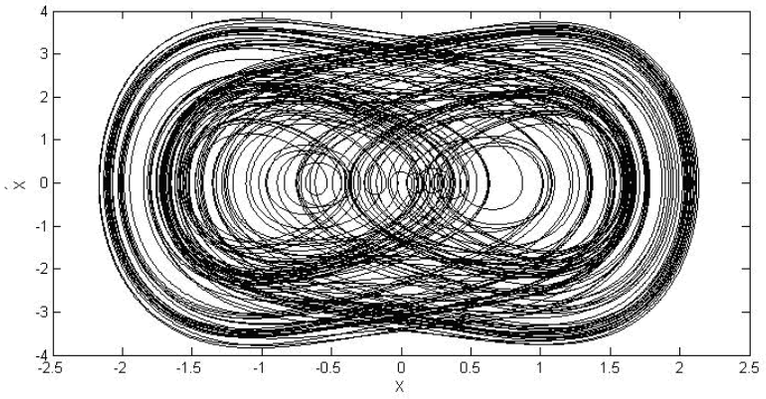

Figure 9. Phase diagram

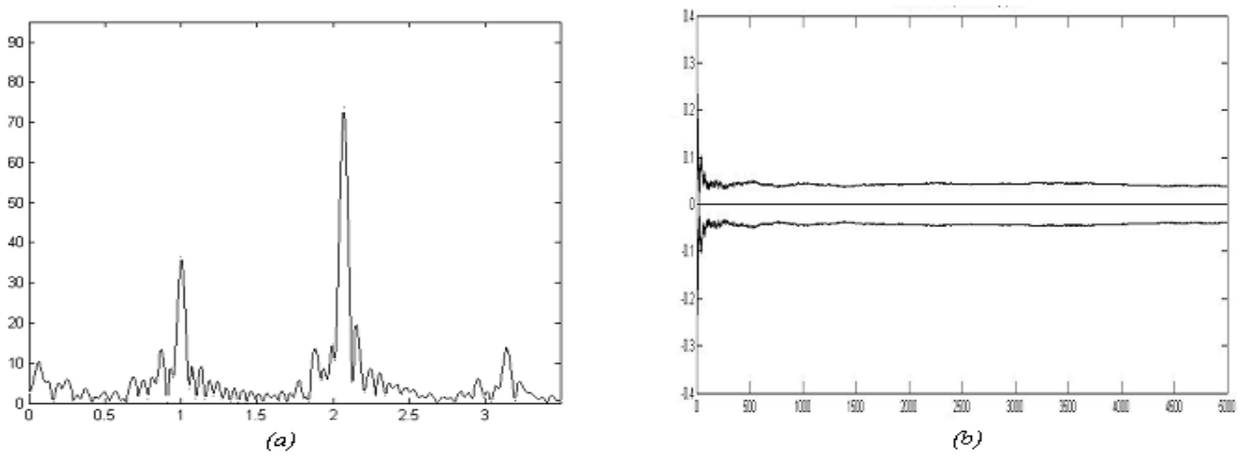

Figure 10. (a): FFT, (b): Lyapunov exponent

5. Chaos with hydrodynamic damping in TM-AFM

The elastic constant of the cantilever k_c must be less than the effective elastic constant of the interatomic coupling k_{at} of the sample. Thus the elastic constant of the spring must be $K < K_{at}$, with $K_{at} = w_{at}^2 m_{at}$. Typical atomic vibration frequencies are $\omega_{at} = 10^{13} Hz$ and atomic masses are of order 10^{-25} kg and $K < 10$ [N / m]. Considering the case of $K < K_{at}$ and rewriting the equation into state space results:

$$\begin{aligned} \dot{x}_1 &= x_2 \\ \dot{x}_2 &= -rx_2 - bx_1 - cx_1^3 - \frac{d}{(a+x_1)^2} + \frac{e}{(a+x_1)^8} + g\cos\Omega x_3 - \frac{p}{(a+x_1)^3} x_2 \end{aligned} \tag{17}$$

where $x_1 = y$, $x_2 = \dot{y}$. The phase diagram can be observed in Figure 11a. For the parameters values: $\Omega = 1$; $r = 0.1$; $b = 0.05$; $c = 0.35$; $d = 4/27$; $e = 0.0001$; $g = 0.2$; $p = 0.005$ and $a = 1.6$. The Lyapunov exponents ($\lambda_1 = -0.23$, $\lambda_2 = 0$; $\lambda_3 = 0.1$), can be seen in Figure 11b, indicating that the system has a chaotic attractor.

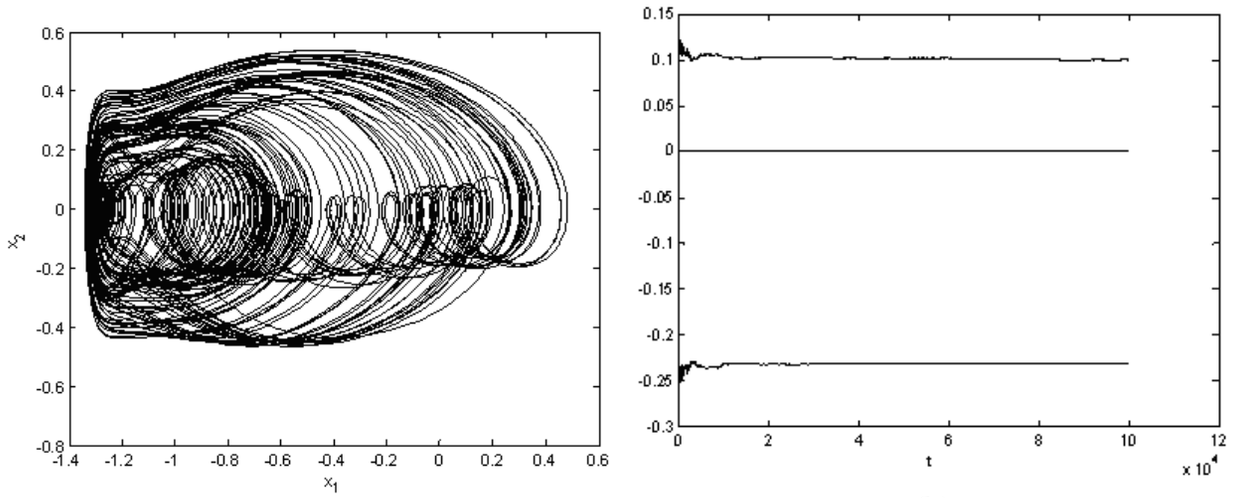

(a) (b)

Figure 11. (a): Phase diagram (b): Lyapunov exponents

6. Scanner position control

A laser beam focus on the top of the microcantilever and the reflection is detected by a photodiode. The light is converted into an electrical signal, and stored in the computer as a reference. An oscillation of the microcantilever deflects the laser beam on the photodiode, allowing the system to compute the microcantilever motion. The error signals are then forwarded, and the piezoelectric scanner moves vertically to scan the sample, as shown in Figure 3. The control techniques are diverse: PID or PD, sliding mode, LQR, or other.

6.1. Feedback control for the model with hydrodynamic damping

Considering the model (17) with the inclusion of control: F_u .

$$\begin{aligned}\dot{x}_1 &= x_2 \\ \dot{x}_2 &= -rx_2 - bx_1 - cx_1{}^3 - \frac{d}{\left(a+x_1\right)^2} + \frac{e}{\left(a+x_1\right)^8} + g\cos\Omega x_3 - \frac{p}{\left(a+x_1\right)^3}x_2 + F_u\end{aligned} \tag{18}$$

and defining a periodic orbit as a function of $\tilde{x}(t)$. The desired regime is given by:

$$\ddot{\tilde{y}} = -r\dot{\tilde{y}} - b\tilde{y} - c\tilde{y}^3 - \frac{d}{\left(a+\tilde{y}\right)^2} + \frac{e}{\left(a+\tilde{y}\right)^8} + g\cos\Omega\tau - \frac{p}{\left(a+\tilde{y}\right)^3}\dot{\tilde{y}} + \tilde{u} \tag{19}$$

Since $\tilde{u}$ control the system in the desired trajectory, and $\tilde{x}(t)$ is a solution of (19), without the term control F_u , then $\tilde{u} = 0$, resulting:

$$\tilde{y} = a_0 + a_1\cos(\Omega\tau) + b_1 sen(\Omega\tau) + a_2\cos(2\Omega\tau) + b_2 sen(2\Omega\tau) + \ldots \tag{20}$$

The feedforward control $\tilde{u}$ is given by:

$$\tilde{u} = \dddot{\tilde{y}} + r\ddot{\tilde{y}} + b\dot{\tilde{y}} + c\tilde{y}^3 + \frac{d}{\left(a+\tilde{y}\right)^2} - \frac{e}{\left(a+\tilde{y}\right)^8} - g\cos\Omega\tau + \frac{p}{\left(a+\tilde{y}\right)^3}\dot{\tilde{y}} \tag{21}$$

Replacing (19) in (18) and defining the deviation from the desired trajectory as:

$$e = \begin{bmatrix} x_1 - \tilde{x}_1 \\ x_2 - \tilde{x}_2 \end{bmatrix} \tag{22}$$

The system (18) can be represented as follows:

$$\begin{aligned} \dot{e}_1 &= e_2 \\ \dot{e}_2 &= -re_2 - be_1 - c\left(e_1 + \tilde{x}_1\right)^3 + c\tilde{x}_1{}^3 - \frac{d}{\left(a+e_1+\tilde{x}_1\right)^2} + \frac{d}{\left(a+\tilde{x}_1\right)^2} + \frac{e}{\left(a+e_1+\tilde{x}_1\right)^8} - \frac{e}{\left(a+\tilde{x}_1\right)^8} - \\ &\frac{p\left(e_2+\tilde{x}_2\right)}{\left(a+e_1+\tilde{x}_1\right)^3} + \frac{p\tilde{x}_2}{\left(a+\tilde{x}_1\right)^3} + u \end{aligned} \tag{23}$$

with $u = F_u - \tilde{u}$, and the feedback control: $u = -Ke$. The system (23) can be represented in deviations as:

$$\dot{e} = Ae + g(x) - g(\tilde{x}) + Bu \tag{24}$$

Representing the system (24) in the form:

$$\begin{bmatrix} \dot{e}_1 \\ \dot{e}_2 \end{bmatrix} = \begin{bmatrix} 0 & 1 \\ -b & -r \end{bmatrix}\begin{bmatrix} e_1 \\ e_2 \end{bmatrix} + g(x) - g(\tilde{x}) + \begin{bmatrix} 0 \\ 1 \end{bmatrix}u \tag{25}$$

where

$$g(x) - g(\tilde{x}) = \begin{bmatrix} 0 \\ -c\left[\left(e_1+\tilde{x}_1\right)^3 - \tilde{x}_1{}^3\right] - \frac{d}{\left(a+e_1+\tilde{x}_1\right)^2} + \frac{d}{\left(a+\tilde{x}_1\right)^2} \end{bmatrix} + \begin{bmatrix} 0 \\ \frac{e}{\left(a+e_1+\tilde{x}_1\right)^8} - \frac{e}{\left(a+\tilde{x}_1\right)^8} - \frac{p\left(e_2+\tilde{x}_2\right)}{\left(a+e_1+\tilde{x}_1\right)^3} + \frac{p\tilde{x}_2}{\left(a+\tilde{x}_1\right)^3} \end{bmatrix}$$

Defining the desired trajectory as the periodic orbit, with amplitude less than (a) and frequency equal to (Ω), then:

$$\tilde{x} = 1.3\sin(t) \tag{26}$$

Considering the parameters values: $\Omega = 1$; $r = 0.1$; $b = 0.05$; $c = 0.35$; $d = 4/27$; $e = 0.0001$; $g = 0.2$; $p = 0.005$ e $a = 1.6$ the matrices A and B, are given by:

$A=\begin{bmatrix} 0 & 1 \\ -0.05 & -0.1 \end{bmatrix}$, $B=\begin{bmatrix} 0 \\ 1 \end{bmatrix}$, and defining $Q=\begin{bmatrix} 10 & 0 \\ 0 & 10 \end{bmatrix}$, $R=\begin{bmatrix} 1 \end{bmatrix}$, and using the matlab(R) the control u is obtained. In Figure 12 the tip displacement without and with control are shown.

$$u=-k_{11}e_1-k_{12}e=-3.1127e_1-3.9293e_2 \tag{27}$$

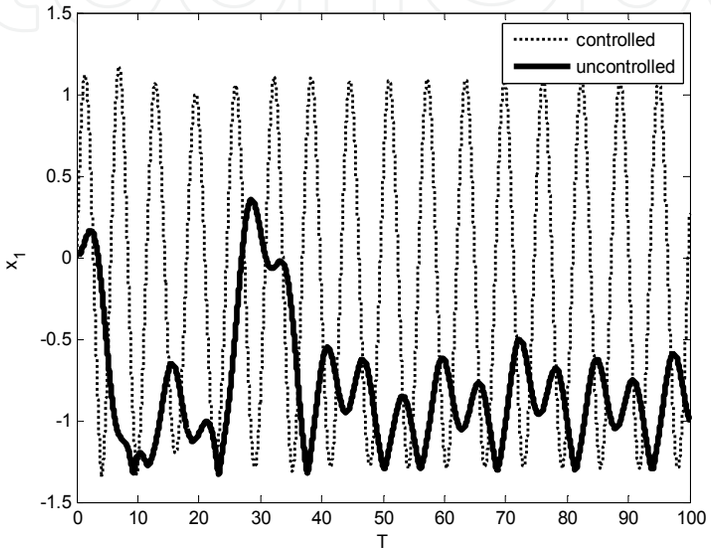

Figure 12. Displacement of the tip to the system without control and with control

6.2. Feedback control for a model with cubic spring

Considering the following parameters: $\alpha=0.14668$, $b=0.17602$, $\delta=2.6364$, $z=2.5$, $a_1=1$, $a_2=14.5$, and the control U in (16) results:

$$\begin{aligned} \dot{x}_1 &= x_2 \\ \dot{x}_2 &= -\alpha a_1 x_1-\beta a_2 x_1^3-\frac{b}{\left(z+x_1\right)^2}+\delta\sin b+U \end{aligned} \tag{28}$$

where: $U=\tilde{u}+u$, u is the feedback control, $\tilde{u}$ is the feedforward control, given by :

$$\tilde{u}=\dot{\tilde{x}}_2+\alpha a_1\tilde{x}_1+\alpha a_2\tilde{x}_1^3+\frac{b}{\left(z+\tilde{x}_1\right)^2}-\delta\sin b \tag{29}$$

Replacing (29) in (28) and defining the deviation from the desired trajectory as:

$$y=(x-\tilde{x}) \tag{30}$$

where $\tilde{x}$ is the desired orbit, and rewriting the system in deviations, results:

$$\dot{y}_1 = y_2$$
$$\dot{y}_2 = -\alpha a_1 y_1 - \alpha a_2 \left(y_1 + \tilde{x}_1\right)^3 + \alpha a_2 \tilde{x}_1{}^3 - \frac{b}{\left(z + y_1 + \tilde{x}_1\right)^2} + \frac{b}{\left(z + \tilde{x}_1\right)^2} + u \tag{31}$$

Considering the system (31) in the following way:

$$\dot{y} = Ay + g(x) - g(\tilde{x}) + Bu \tag{32}$$

where: $y = \begin{bmatrix} y_1 \\ y_2 \end{bmatrix}$; $A = \begin{bmatrix} 0 & 1 \\ -\alpha a_1 & 0 \end{bmatrix}$; $B = \begin{bmatrix} 0 \\ 1 \end{bmatrix}$ and

$g(x) - g(\tilde{x}) = \begin{bmatrix} 0 \\ -\alpha a_2 \left(y_1 + \tilde{x}_1\right)^3 + \alpha a_2 \tilde{x}_1{}^3 - \frac{b}{\left(z + y_1 + \tilde{x}_1\right)^2} + \frac{b}{\left(z + \tilde{x}_1\right)^2} \end{bmatrix}$. The control u is obtained by solving the following equation:

$$u = -R^{-1} B^T P y \tag{33}$$

where P is a symmetric matrix, solution of the reduced Riccati equation:

$$PA + A^T P - PBR^{-1} B^T P + Q = 0 \tag{34}$$

Defining the desired trajectory as:

$$\tilde{x} = 2\cos(t) \tag{35}$$

The matrices $A = \begin{bmatrix} 0 & 1 \\ -0.14668 & 0 \end{bmatrix}$, $B = \begin{bmatrix} 0 \\ 1 \end{bmatrix}$, and defining Q and R as $Q = \begin{bmatrix} 250 & 0 \\ 0 & 20 \end{bmatrix}$, $R = \begin{bmatrix} 0.1 \end{bmatrix}$, results after using the matlab(R) to obtain u:

$$u = -49.8535 y_1 - 17.3120 y_2 \tag{36}$$

In Figure 13 it can observed the tip displacement with and without control.

7. AFM mathematical modeling with Phase-Locked Loops (PLLS)

As mentioned above, the Atomic Force Microscopy started in 1986 when the Atomic Force Microscope (AFM) was invented by Binnig in 1986. Since then many results have been obtained by simple contact measurements. However, the AFM cannot generate truly atomic resolution images, by simple contact measurement, in a stable operation. Besides, since 1995, using noncontact techniques, it was possible to obtain atomic resolution images, with stable operation, under attractive regime at room temperature (Giessible, 1995; Morita et. al., 2009). Noncontact AFM operates in static and dynamic modes. In the static mode the tip-sample interaction forces are translated into measured microcantilever deflections, and the image is a map z(x,y,F_{ts}) with F_{ts} constant.

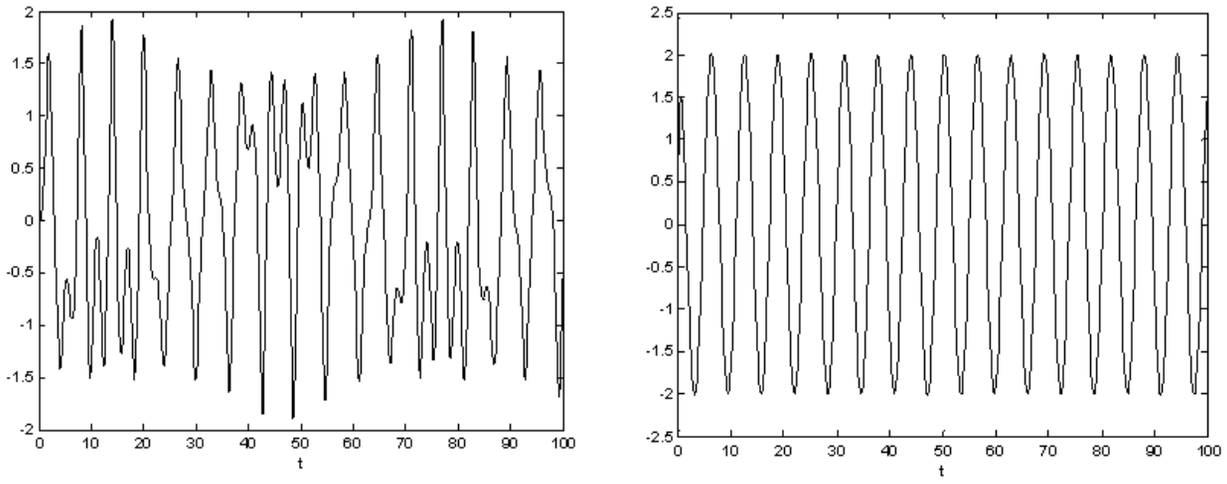

(a) (b)

Figure 13. (a): Tip displacement without control (b): Tip Displacement with control

In the dynamic mode the microcantilever is deliberately vibrated. The Amplitude Modulated AFM and the Frequency Modulated AFM are the most important techniques. In both AM-AFM and FM-AFM the amplitude and frequency of the microcantilever are kept constant by two control loops. The AGC (Automatic Gain Control) and the ADC (Automatic Distance Control). The AGC controls the amplitude of oscillation and the ADC controls the frequency by adjusting the distance between tip and sample. The oscillatory behavior of the microcantilever is illustrated in Figure 14. The FM-AFM block is shown in Figure 15.

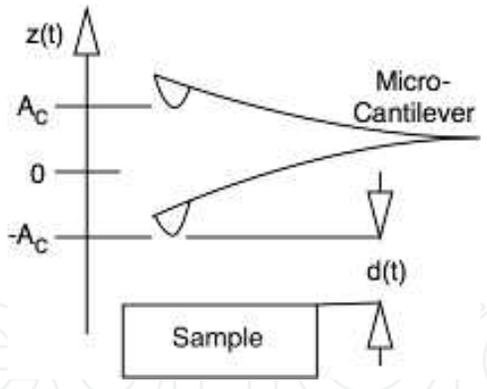

Figure 14. Microcantilever oscillatory behavior. Source: (Bueno et al., 2011).

In the FM-AFM the control signal of the AGC loop is used to generate the dissipation images and the ADC control signal is used to generate the topographic images. The FM-AFM improved image resolution and for surface studies in vacuum is the preferred AFM technique (Morita et. al., 2009; Bhushan, 2004). From Figure 15 it can be seen that the PLL generates the feedback signal for both control loops, therefore the PLL performance is vital to the FM-AFM. The PLL is a closed loop control system that synchronizes a local oscillator to a sinusoidal input. The PLLs are composed of a phase detector (usually a multiplier circuit), of a low-pass filter and of a VCO (Bueno et. al., 2010; Bueno et al., 2011), as it can be seen in Figure 16, and additionally, shows the PM and AM outputs used in the AFM system.

The AGC loop also depends on the amplitude detector output, shown in Figure 17. The amplitude detector is composed of diode followed by a first-order low-pass filter. The circuit holds the output A(t) for a while, allowing the AGC to determine the control signal.

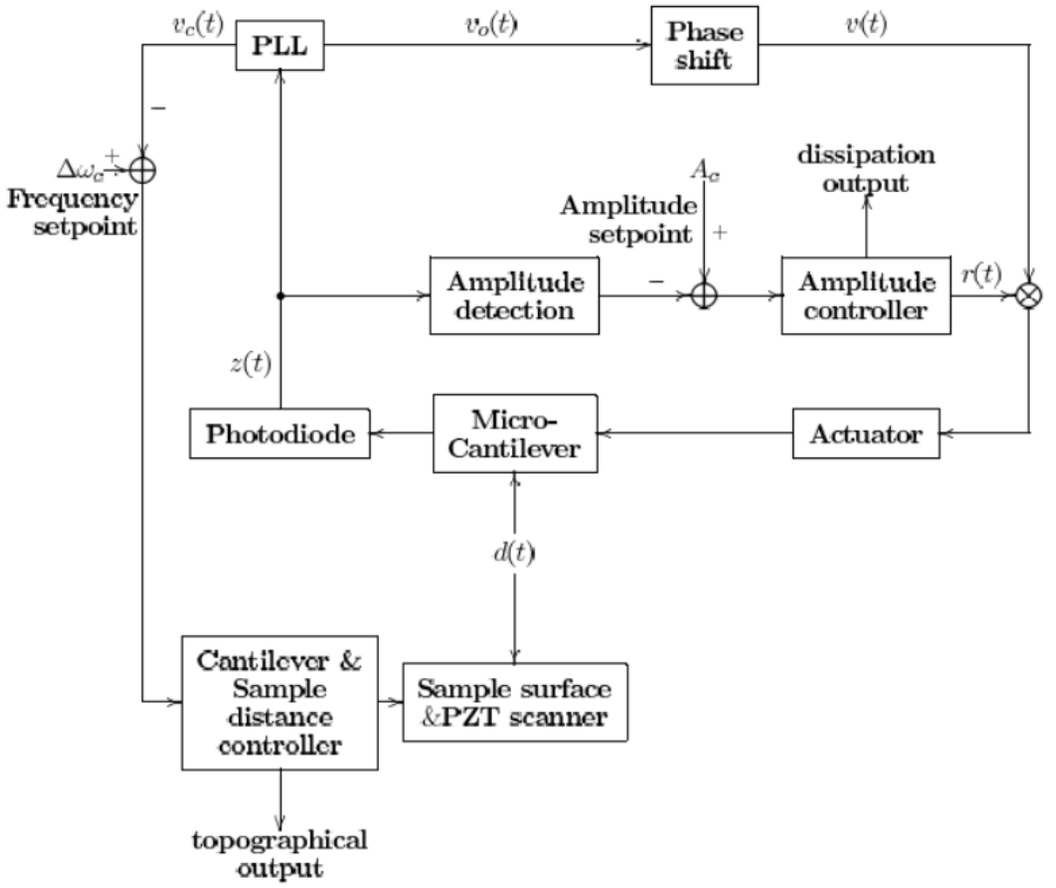

Figure 15. Block Diagram of the FM-AFM control system. Source: (Bueno et al., 2011).

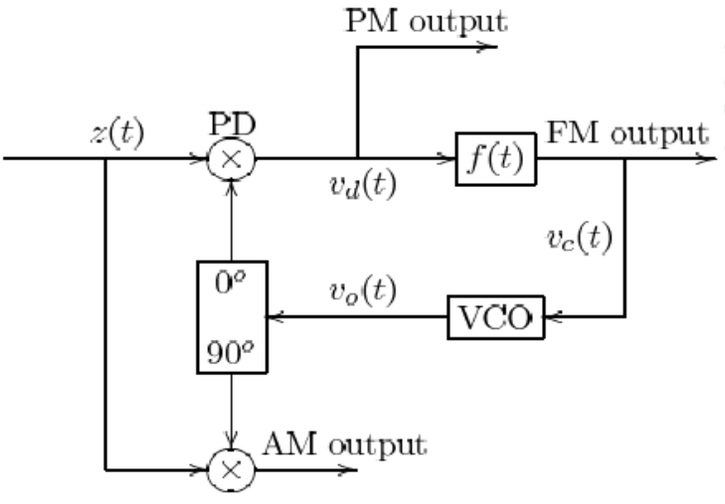

Figure 16. PLL block diagram

7.1. Mathematical model of the FM-AFM

The mathematical model of the FM-AFM considers the microcantiler dynamics, the tip-sample interaction, the amplitude detector circuit and the PLL. The microcantilever is assumed to be a second order system with natural frequency ω_c and damping coefficient γ. Concerning to tip-sample interaction, there are short, medium and long range forces. Since the FM-AFM operates in long-range distance, the predominant force is the Van Der Waals $\frac{A_H}{6\left(d(t)+z(t)\right)^2}$, where A_H is the Hamaker constant and d(t) is the tip-sample distance, Figure 7.1. Besides, the microcatilever is excited by an external forcing signal with a previously determined amplitude. The signal is a sinusoid with phase $\omega_c t+\varphi(t)$ and amplitude $r(t)v_o$, where $r(t)$ is the AGC signal, and v_o is constant. The tip-sample interaction forces cause modulations both in the amplitude and in the frequency of oscillation of the AFM microcantilever. The modulations are detected by the PLL and used by the AGC and by the ADC, in order to control the microcantilever, drivin it to oscillate according to $z\left(t\right)=A\left(t\right)sen\left(\omega_c t+\varphi_c\left(t\right)\right)$. The microcantilever mathetamical model is given by equation 37.

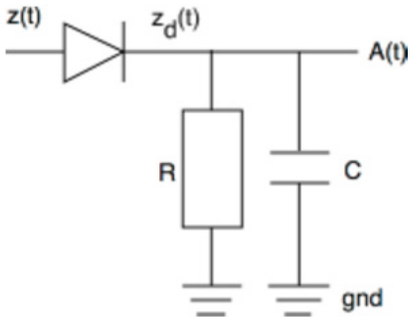

Figure 17. Amplitude detector. Source (Bueno et al., 2011)

The mathematical model of the amplitude detector is given by equation 38, where $\tau_d=\frac{1}{RC}$ and $z_d=\begin{cases}z(t), & z(t)>0\\ 0, & z(t)\le 0\end{cases}$. The PLL model can be seen in many works in the literature. The mathematical model in equation 39 follows Bueno et al., 2010 and 2011. Considering the filter transfer function $f\left(t\right)=\frac{\alpha_0}{s^2+\beta_1 s+\beta_0}$ and the gain $G=\frac{1}{2}k_m k_o v_o A_c$, where k_m is the phase detector gain, k_o is the VCO gain, v_o is the VCO output amplitude and A_c is the nominal microcantilever amplitude of oscillation, Figure 14. Equations 40 and 41 represent the AGC and ADC, respectively. Equations 37 to 41 are the model of the FM-AFM.

$$\ddot{z}+\gamma\dot{z}(t)+\omega_c^2 z(t)=r(t)v_o sen\left(\omega_c t+\varphi_o\left(t\right)\right)+\frac{A_H}{6\left(d(t)+z(t)\right)^2} \tag{37}$$

$$\dot{A}(t) + \tau_d A(t) = \tau_d z_d(t) \tag{38}$$

$$\dddot{\varphi}_o(t) + \beta_1 \ddot{\varphi}_o(t) + \beta_0 \dot{\varphi}_o(t) + \alpha_0 G sen\left(\varphi_o(t) - \varphi_c(t)\right) = 0 \tag{39}$$

$$r(t) = \Phi_{AGC}\left(A_c - A(t)\right) \tag{40}$$

$$d(t) = \Phi_{ADC}\left(\Delta\omega_c - \dot{\varphi}_o(t)\right) \tag{41}$$

7.2. Local stability and PLL design for FM-AFM

From equation 39, and considering the phase error $\vartheta = \varphi_o - \varphi_c$, results that:

$$\dddot{\vartheta} + \beta_1 \ddot{\vartheta} + \beta_0 \dot{\vartheta} + \alpha_0 G sen(\vartheta) = \dddot{\varphi}_c + \beta_1 \ddot{\varphi}_c + \beta_0 \dot{\varphi}_c \tag{42}$$

that represents the phase erros between the microcantilever oscillation and the PLL. The PLL behavior analysis is conveniently perfomed considering the cylindric state space, considering $\vartheta \in (-\pi, \pi]$. In that case, the synchronous state, corresponding to an asymptocally stable equilibrium point of equation 42 (See Bueno et al., 2010 and Bueno et al., 2011), corresponds to a Constant phase error ϑ and to null frequency and acceleration errors, i.e., $\dddot{\vartheta} = \ddot{\vartheta} = \dot{\vartheta} = 0$. For small phase erros it can be considered that $sen(\vartheta) \approx \vartheta$ in (42). In addition, considering $\varphi_c = \Omega t$, (42) can be rewritten as:

$$\dddot{\vartheta} + \beta_1 \ddot{\vartheta} + \beta_0 \dot{\vartheta} + \alpha_0 G \vartheta = \beta_0 \Omega \tag{43}$$

that represents the PLL linear response to a frequency shift (step) of amplitude Ω. The local stability of equation 42 can be determined by the position of the poles of equation 43, or by the Routh-Hurwitz criterion (See Bueno et al., 2010 and Bueno et al., 2011; Ogata, 1993). Therefore, considering that the coefficients of the filter are all positive and real, the poles of equation 43 have negative real parts if:

$$G < \frac{\beta_0 \beta_1}{\alpha_0}. \tag{44}$$

Considering the filter coefficients $\alpha_0 = \beta_0 = \omega_n^2$ and $\beta_1 = 2\xi\omega_n$, where ξ is the damping factor and ω_n the natural frequency, then, from equation 44, results:

$$G < 2\xi\omega_n. \tag{45}$$

Equation 45 establishes a design criterion that assure the local stability of the PLL, i.e., for small phase and frequency steps the PLL synchronizes to the microcantilever oscillation. Additionally, from the design parameters ξ and ω_n the loop gain G has a superior bound, and can be determined in order to satisfy the requirements of performance and stability.

Despite the good transient response and high frequency noise rejection - such as the double frequency jiter -, provided by the all pole filter the steady state response may need improvement. The PLL must demodulate an FSK (Frequency Shift Keying) signal, that actually is a frequency step. In order to track a frequency shift the loop filter must have at least a pure integration, i.e., the PLL must be at least a type 2 system (Bueno et al., 2010 and Bueno et al., 2011; Bueno, 2009, Ogata, 1993). According to that, and considering the loop filter $F(s) = \frac{as+1}{s(bs+1)}$ the stability of the PLL is assured only if $a > b$.

Figure 18 illustrates the PLL response to an FSK signal, showing the PLL FM output (figure 16). After the transient the mean value of the FM output is the same value of the FSK signal. The oscillation is due to the Double frequency jitter (Bueno et al., 2010 and Bueno, 2009). This shows that the PLL design must provide strong damping to noise and to the double frequency jitter. Besides, if the PLL is not at least of type 2 the PLL presents steady state error in the FSK demodulation, impairing the AFM imaging process. The PLL perfomance was analysed and presented under the FM-AFM perspective. Besides, a PLL design method was shown and illustrated by simulation, making clear the PLL performance importantance in the AFM control system.

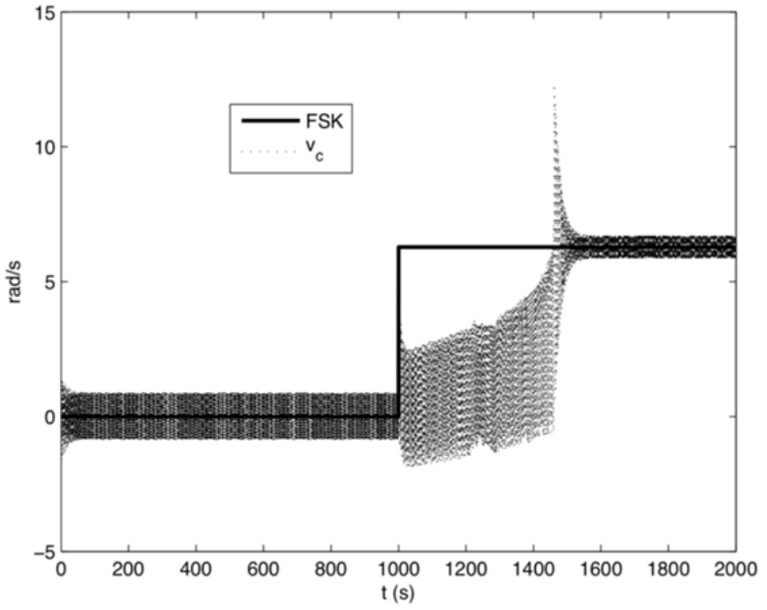

Figure 18. PLL response to a FSK signal.

8. Conclusions

This chapter deals with emergent problems in the Engineering Science research, presenting study and research related to NEMS systems, specially microcantilevers with many modes of vibration, for which the tip-sample interaction forces are highly nonlinear, impairing the stability of the latent image, while the others modes of vibration can be explored in order to improve the AFM performance.

In the context of this work, the following specific problem have been approached: The understanding of the relations of the properties and the structure of the nanoscopic and molecular materials, through the atomic force microscopy, using microcantilevers, giving subsidiary information to next generation of microscopy instrumentation.

Author details

José Manoel Balthazar
UNESP - Univ Estadual Paulista, Rio Claro, SP, Brasil
UNESP - Univ Estadual Paulista Paulista, Bauru, SP, Brasil

Angelo Marcelo Tusset and Atila Madureira Bueno
UTFPR - Universidade Técnica Federal do Paraná, Ponta Grossa, PR, Brasil

Bento Rodrigues de Pontes Junior
UNESP - Univ Estadual Paulista Paulista, Bauru, SP, Brasil

9. References

[1] Awrejcewicz, J. Bifurcation and Chaos in Coupled Oscillators. World Scientific, Singapore, 1991.

[2] Awrejcewicz, J., Lamarque, C.H. Bifurcation and Chaos in Nonsmooth Mechanical Systems. World Scientific Publishing, Singapore 2003.

[3] Alves, J.R.; Pontes Junior, B.R.; Balthazar, J.M., Modeling and dynamics of an electromechanical absorber applied to vibration control: performance and limitations. 21st Brazilian Congress of Mechanical Engineering, October 24-28, 2011, Natal, RN, Brazil, 2011.

[4] Alves, J.R. & Pontes Junior, B.R., "Modelagem e Dinâmica de um Absorvedor Eletromecânico Aplicado no Controle de Vibrações." (Relatório de Pesquisa - FAPESP), Departamento de Engenharia Mecânica, Faculdade de Engenharia, UNESP, Bauru. 2011. 70p.

[5] Alves, J.R., Pontes Junior, B.R., Modelagem e dinâmica de um absorvedor eletromecânico aplicado no controle de vibrações. ANAIS do CIC2010 - Congresso de Iniciação Científica da UNESP, Bauru, p. 1-4, 2010

[6] Anton, S.R. and Sodano, H.A. 2007. ''A Review of Power Harvesting Using Piezoelectric Materials (2003—2006),'' Smart Mater. Struct., 16:R1 R21.

[7] Ashhab M, Salapaka MV, Dahleh M, Mezic I. Dynamical analysis and control of microcantilevers. Automatica 1999; 35:1663–70.

[8] Ashhab M, M. V. Salapaka, M. Dahleh, I. Mezic, "Melnikov-based dynamical analysis of microcantilevers in scanning probe microscopy", Nonlin. Dyn, 20, 197-220. 1999.

[9] Binnig, G.: Atomic Force Microscope and Method for Imaging Surfaces with Atomic Resolution. US Patent. n: 4, 724, 318, (1986).

[10] Binnig, G., Gerber, Ch., Quate, C. F.: Atomic Force Microscope. Phys. Rev. Lett. 56, pp: 930-933, (1986).

[11] Beeby, S.P., Tudor, M.J., White, N.M., "Energy harvesting vibration sources for microsystems applications", Measurement Science and Technology 17, 2006, pp 175-195
[12] Bishop, R. H. The Mechatronics Handbook, CRC Press, 2002, ISBN: 0849300665.
[13] Bowen, W.R.; Hilal, N., Atomic Force Microscopy in Process Engineering - An Introduction to AFM for Improved Processes and Products, Elsevier, 2009.
[14] Bhushan, B; Handbook of Nanotechnology, Springer, Berlin, 2004.
[15] Bueno, A.M.; Ferreira, A. A.; Piqueira, J.R.C.; Modeling and Filtering Double-Frequency Jitter in One-Way Master Slave Chain Networks. Circuits and Systems I: Regular Papers, IEEE Transactions on 57 3104 -3111, 2010.
[16] Bueno, A. M.; Balthazar, J. M.; Piqueira, J. R. C. Phase-Locked Loop design applied to frequency-modulated atomic force microscope. Communications in Nonlinear Science and Numerical Simulation, (16)3835 – 3843, 2011.
[17] Bueno, A.M.; Ferreira, A. A.; Piqueira, J.R.C.; Modeling and measuring. Communications In Nonlinear Science and Numerical Simulation 14 1854-1860, 2009.
[18] Cidade, G. A. G.; Silva Neto, A. e Roberty, N. C Restauração de Imagens com Aplicações em Biologia e Engenharia: Problemas Inversos em Nanociência e Nanotecnologia Notas em Matemática Aplicada; 3 - Sao Carlos, SP : SBMAC, 2003, xiv, 88 p.
[19] Chtiba, M. O., Choura, S., Nayfeh, A.H., El-Borgia, S. 2010.Vibration confinement and energy harvesting in flexible structures using collocated absorbers and piezoelectric devices, Journal of Sound and Vibration 329 (2010) 261–276.
[20] Cottone, F., 2007, "Nonlinear Piezoelectric Generators for Vibration Energy Harvesting", Universita' Degli Studi Di Perugia, Dottorato Di Ricerca In Fisica, XX Ciclo.
[21] De Marqui Jr, C., Erturk, A., Inman, D. J. 2009. An electromechanical finite element model for piezoelectric energy harvester plates, Journal of Sound and Vibration 327 (2009) 9–25.
[22] Du Toit, N.E. and Wardle, B.L. 2007. ''Experimental Verification of Models for Microfabricated Piezoelectric Vibration Energy Harvesters,'' AIAA Journal, 45:1126—1137.
[23] De Martini, B.E., Rhoads, J.F., Turner, K.L., Shaw, S.W., Moehlis, J., "Linear and Nonlinear Tuning of Parametrically Excited MEMS Oscillators" in Journal of Microelectromechanical Systems, vol. 16, no. 2, 2007, pp 310-318
[24] Erturk, A., Inman, D.J., "On mechanical modeling of cantilevered piezoelectric vibration energy harvesters", Journal of Intelligent Material Systems and Structures, 2008
[25] Halliday, D., Resnick, R., Walker, J., Fundamentals of Physics, v. 3, 7th ed, Jonh Wiley and Sons, 2005.
[26] Felix, Jl.P. and Balthazar, J.M, Comments on a nonlinear and nonideal electromechanical damping vibration absorber, Sommerfeld effect and energy transfer. Nonlinear Dynamics, (2009) Volume 55, Numbers 1-2, 1-11, DOI: 10.1007/s11071-008-9340-8
[27] Farrokh, A., Fathipour, M., Yazdanpanah, M.J., High precision imaging for noncontact mode atomic force microscope using an adaptive nonlinear observer and output state

feedback controller, Digest Journal of Nanomaterials and Biostructures Vol. 4, No.3, September 2009, p. 429-442.

[28] Garcia, R., Pérez, R.: Dynamic atomic force microscopy method. Surface Science Report, 47, pp: 197-301, (2002).

[29] Garcia, R., San Paulo, A.: Dynamics of a vibrating tip near or in intermittent contact with a surface. Physical Review B, 61, pp: R13381-R13384, (2000).

[30] Giessibl, F. Atomic Resolution of the Silicon (111)-(7x7) Surface by Atomic Force Microscopy. Science 267 68--71 1995.

[31] Hu, S., Raman, A.: Analytical formulas and scaling laws for peak interaction forces in dynamic atomic force microscopy. Applied Physics Letters, 91, pp: 123106(1-3), (2007).

[32] Iossaqui, J. G., Uso de Absorvedores de Vibrações Eletromecânicos Lineares e Não-Lineares em Sistemas Não-Lineares e Não-Ideais, Bauru: Faculdade de Engenharia, UNESP-Universidade Estadual Paulista, 2009, 106 p., Dissertação (Mestrado).

[33] Iossaqui, J. G.; Balthazar, J. M.; Pontes, B. R. J; Felix, J. L. P.. Atuação de Absorvedores Eletromecânicos de Vibrações Não-Lineares e Não-Ideais. In: V Congresso Nacional de Engenharia Mecânica (CONEM 2008), 2008, Salvador. Anais do V Congresso Nacional de Engenharia Mecânica (CONEM 2008). Rio de Janeiro : ABCM, 2008-a. v. 1. p. 1-10.

[34] Iossaqui, J. G.; Balthazar, J. M.; Pontes, B. R. J; Felix, J. L. P.. On a Passive Control in a Nonlinear and a Nonideal System. In: 7º Congresso Temático de Dinâmica, Controle e Aplicações - DINCON 2008, 2008, Presidente Prudente. Anais do 7º Congresso Temático de Dinâmica, Controle e Aplicações - DINCON 2008. São Carlos : SBMAC, 2008-b. v. 1. p. 1-6.

[35] Iossaqui, J. G., Balthazar, J. M.;; Pontes, B. R. J; Felix, J. L. P.. Suppresing Chaotic Behaviour in A Double-Well Oscillator with Limited Power Supply Using Eleteromechanical Damper Device. In: Joint Conference on Mechanics and Materials, 2009, Blacksburg, VA. Proceedings of 2009 Joint Conference on Mechanics and Materials. Blacksburg : Virginia TECH, 2009.

[36] Jalili, N., Laxminarayana,K. A review of atomic force microscopy imaging systems: application to molecular metrology and biological sciences. Mechatronics 14:8, 907–945. 2004.

[37] Jalili, N.; Dadfarnia, M.; Dawson, D. M.; Distributed parameters base modeling and vibration analysis of microcantilevers used in atomic force microscopy, Proceedings of the ASME 2009 International Design Engineering Technical Conferences & Computers and Information in Engineering Conference, IDETC/CIE 2009, August 30 - September 2, 2009, San Diego, California, USA

[38] Krylov, S., Harari, I., Cohen, Y., "Stabilization of electrostatically actuated microstructures using parametric excitation", Journal of Micromechanics and Microengineering 15, 2005, pp 1188–1204

[39] Kuroda,M, H. Yabuno, K. Hayshi, K. Ashida, "Amplitude Control in a van der Pol-Type Self-Excited AFM Microcantililever", Journal of System Design and Dynamics. Vol. 2, n. 3, 2008.

[40] Liu, S., Davidson, A., Lin, Q., "Simulation studies on nonlinear dynamics and chaos in a MEMS cantilever control system" in Journal of Micromechanics and Microengineering 14, 2004, pp 1064–1073
[41] Moon, F. C. Chaotic and Fractal Dynamics, New Jersey: Wiley, 1992
[42] Moon, F.C., 1998, "Applied Dynamics: With Applications to Multibody and Mechatronic Systems", Ed. Wiley-Interscience, Canada, 492 p
[43] Lennard-Jones, J. E. (1924), "On the Determination of Molecular Fields", Proc. R. Soc. Lond. A 106 (738): 463–477, doi:10.1098/rspa.1924.0082.
[44] Lozano, J. R., Garcia, R.: Theory of Multifrequency Atomic Force Microscopy. Physical Review Letters. PRL 100, pp: 076102(1-4), (2008).
[45] Mauricio, M. H. P.: Microscopia de Ponta de Prova (Scanning Probe Microscopy): AFM - Microscopia de Força Atômica (2011)
http://www.dema.pucrio.br/cursos/micquant/SPM.pdf, acesso em 10 de Fev., 2011.
[46] Morita, S.; Wiesendanger, R.; Meyer, E.; Giessibl, F. J.; Noncontact atomic force microscopy, Berlin:Springer, 2009.
[47] Ogata, K; Engenharia De Controle Moderno.1993.
[48] Preumont, A. Mechatronics Dynamics of Electromechanical and Piezoelectric Systems. Netherlands: Springer, 1999.
[49] Priya, S., Inman, D.J. 2009 Energy Harvesting Technologies, Springer Science Business Media, LLC 2009.
[50] Paulo, A.S., R. Garcia, "Unifying theory of tapping-mode atomic-force microscopy", Phys. Rev. B 66, 041406 (R), 2002.
[51] Quinn, D.D., Vakakis, A.F., Bergman, L.A., "Vibration-based energy harvesting with essential nonlinearities" in Proceedings of the ASME International Design Engineering Technical Conferences & Computers and Information in Engineering Conference, 2007
[52] Raman, A., Melcher, J., Tung, R.: Cantilever Dynamics in Atomic Force Microscopy. Nanotoday, vol: 3, pp: 20-27, (2008).
[53] Rafikov, M., Balthazar J. M., 2008. "On control and synchronization in chaotic and hyperchaotic systems", Communications in Nonlinear Science & Numerical Simulation, vol: 13, pp. 1246-1255.
[54] Roundy, S., Wright, P.K., Rabaey, J., "A study of low level vibrations as a power source for wireless sensor nodes", Comput. Commun. 26 (2003) 1131–1144.
[55] Richard W., B. And Nidal H. Microscopy in process engineering, An introdution to afm for improved processes and products, Elsevier; 2009 USA.
[56] Rutzel, S.; Lee, S. I.; Raman, A. Nonlinear dynamics of atomic-force-microscope probes driven is Lennard-Jones potentials. Proc. R. Soc. Lond, 459, 1925-1948, 2003
[57] Salvadori, M. C. B. S.: Microscopia de Força Atômica e Tunelamento. (2010) http://fluidos.if.usp.br/v1/iiiev/msalvadori_imfcx08.pdf, last accessed March 10, 2010
[58] Sebastian A., A. Gannepalii, M. V. Gannepali. M. V. Salapka. A review of the systems approach to the analysis of dynamic-mode atomic force microscopy. IEEE Transactions on Control Systems Technology, 15(15), 952- 959 (2007).
[59] Sinclair, I. R., Sensors and Transducers 3º ed, New York: Butterworth-Heinemann, 2001.

[60] Sodano, H.A., Inman, D.J., Park, G., "Comparison of piezoelectric energy harvesting devices for recharging batteries", Journal of Intelligent Material Systems And Structures, Vol. 16, 2005

[61] Sodano, H.A., Inman, D.J. and Park, G. 2004. ''A Review of Power Harvesting from Vibration Using Piezoelectric Materials,'' Shock Vib. Dig., 36:197—205.

[62] Sodano, H.A., Park, G. and Inman, D.J. 2004. ''Estimation of Electric Charge Output for Piezoelectric Energy Harvesting,'' Strain, 40:49 58.

[63] Triplett, A., Quinn, D. D. 2008. The Role of Non-Linear Piezoelectricity in Vibration-based Energy Harvesting, Twelfth Conference on Nonlinear Vibrations, Stability, and Dynamics of Structures—June 1–5, 2008.

[64] Triplett, A., Quinn, D. D. 2009. The Effect of Non-linear Piezoelectric Coupling on Vibration-based Energy Harvesting Journal of Intelligent Material Systems and Structures, Vol. 20 p. 1959-1967—November 2009.

[65] Twiefel, J., Richter, B., Sattel, T. And Wallaschek, J. 2008. ''Power Output Estimation and Experimental Validation for Piezoelectric Energy Harvesting Systems,'' J. Electroceram., 20:203—208.

[66] Zanette, S. I.; Funcionamento de um microscópio de força atômica.Notas do curso ministrado no CBPF,1997. DCP/Centro Brasileiro de Pesquisas Físicas/MCT,1997.

[67] Zhang, W.M.; Meng, G., Zhou, J. B.; Chen, J. Y. Nonlinear Dynamics and Chaos of Microcantilever-Based TM-AFMs with Squeeze Film Damping Effects. Sensors, 9, 3854-3874, 2009.

[68] Wang,C.C., N. S. Pai and H. T. Yau. "Chaos control in AFM system using sliding mode control backstepping desing", Comun Nonlinear Sci Numer Simulat, pp 1-11, 2009

[69] Wiesenganger, R. "Scanning probe microscopy and spectroscopy", Great Britain: Canbridge University Press, 1994.

[70] Yamapi, R. Dynamics and sychronization of electromechanical devices with a Duffing nonlinearity. Ph.D. Thesis, University of Abomey-Calavi, Bénin, 2003.